A Numerical Investigation of the Multiphase Filtration Process Considering Medium and Phase Compressibility

Zokhidjon Kaytarov
Samarkand State University, Samarkand, Uzbekistan
z.qaytarov@gmail.com (corresponding author)

Vladimir Burnashev
Samarkand State University, Samarkand, Uzbekistan
vladimir.burnash@mail.ru

Bekzodjon Fayziev
Samarkand State University, Samarkand, Uzbekistan
fayzievbm@mail.ru (corresponding author)

Zuraida Alwadood
Department of Mathematical Sciences, College of Computing, Informatics and Mathematics, Universiti Teknologi MARA (UiTM) Shah Alam, Selangor, Malaysia
zuraida794@uitm.edu.my

Azamat Jumayev
Termez University of Economics and Service, Termez, Uzbekistan
azamatjumayev20.06.1993@gmail.com

Odil Khaydarov
Samarkand State University, Samarkand, Uzbekistan | University of Economics and Pedagogy, Karshi, Uzbekistan
haydarov-odil@samdu.uz

Gafur Namazov
Termez University of Economics and Service, Termez, Uzbekistan
malikberdiyev1975@gmail.com

Received: 15 August 2025 | Revised: 25 September 2025 and 29 October 2025 | Accepted: 31 October 2025

 DOI: https://doi.org/10.48084/etasr.14097

ABSTRACT

This study developed a mathematical model of the multiphase filtration process in a porous medium, accounting for medium and phase compressibility. The problem was solved numerically using the "large particle" method, and the resulting pressure, velocity, porosity, and permeability values were analyzed. The results indicated that during the filtration process with high compressibility, porosity and permeability, a decrease in the bottom-hole zone occurred as reservoir pressure also decreased. This reduction slowed the pressure drop and prevented the filtration process from reaching the far zones of the medium. Consequently, although porosity and permeability were decreased in the bottom-hole zone, their changes were minimal in regions far from the well. The results were validated by comparing the average pressures with those from a previous study, showing good agreement.

Keywords-multiphase filtration; compressible fluid; medium compressibility; porous medium; mathematical model

I. INTRODUCTION

Mathematical modeling of multiphase filtration processes, such as the multiphase filtration of salt water and gas through a saline medium, is one of the most complicated research fields as it requires separate equations for each phase and accounting for the interactions among them [1]. Saline media are suitable for nuclear waste containment because of their low permeability, self-sealing of natural defects, easiness of excavation and massive formation [2]. Using the numerical simulation of the steam-liquid multiphase process, various cleaning scenarios are investigated. For example, a two-phase flow was mathematically modeled considering the phase compressibility [1]. Lift forces were added to the conservation equations written in Baer-Nunziato form [3, 4]. To numerically analyze the process of compressible two-phase fluid filtration, a modified adaptive method of minimum amendments method was utilized in [5]. Additionally, an experimental investigation was carried out to measure the velocity of multiphase flow in pipes utilizing the Electrical Capacitance Tomography [6]. In [7], a flow of gas mixture and unitary fuel particle phases was numerically studied by examining the effects of the diameter of the pipeline and nonhomogeneous distribution of the concentration of particles on spreading detonation waves in gas suspensions.

During the filtration or mass transfer processes, most of the porous media are prone to deformation [8]. Therefore, accounting for medium deformation is important to effectively model the real filtration and transport processes in a porous medium. In [9], the process of fluid filtration from a point source into an isotropic and linearly elastic porous layer was mathematically modeled and analytically solved. Similarly, the process of fluid filtration to horizontal wells in a porous medium was studied in [10], with the medium considered as deformable and transversely isotropic. The stress-strain state of the anisotropic medium and the effect of filtration coefficient on the production of the horizontal well were also investigated. Authors in [11], researched both experimentally and theoretically the effect of viscous drag impartation on the solid during the fluid filtration in a compressible porous medium.

Authors in [12], modeled a viscous compressible fluid filtering through a deformable medium with predominantly viscous properties, incorporating fluid compressibility and gravitational effects. In [13], a dispersion-diffusion of two miscible incompressible fluids in a deformable porous medium was studied including fluid-fluid interactions. The effect of medium compressibility on flow velocities and medium properties was examined, and the solution was obtained through the finite element method based on the quasi-compressibility approach.

In order to solve the fluid filtration problems in deformable media many approaches have been proposed. In [14], an analytical solution was obtained by solving the problem of airflow in a human lung medium. Moreover, a model was developed and solved to simulate subcutaneous injections and subterranean soil flows [9]. To reduce a system of equations for the two-dimensional incompressible fluid model, Lagrange transforms and the method of Runge-Kutta were applied [15]. The Finite difference method was utilized to solve the problem of fluid filtration in a deformable rock layer [8], and multiphase multicomponent flow of a fluid in incompressible porous medium. Numerical analysis of the multiphase filtration process in incompressible porous medium was conducted using modified adaptive minimum amendments methods [6], the "black oil" model [16], the "large particle" method [7], and finite volume shock-capturing techniques [1]. When medium deformation was included, multiphase filtration processes were numerically studied using the finite element method [13, 17] and element-free Galerkin method [18]. In [19], the "large particle" method was extended to analyze the model incompressible multiphase filtration by considering medium deformation.

In this paper, the process of multiphase filtration in a compressible porous medium considering phase compressibility is numerically investigated using the method of "large particle".

II. PROBLEM STATEMENT AND MATHEMATICAL MODEL

A section of an oil reservoir with a single production well was considered. Due to the difference in reservoir and well pressures, the filtration process occurred in the medium. Oil and water phases were assumed to participate in the filtration process. It was also assumed that the phases are immiscible, do not exchange mass, do not change phases, and capillary forces are neglected. The bottom-hole zone was considered symmetric with respect to the well. For this reason, a one-dimensional model was constructed instead of a three-dimensional one.

The equations of the one-dimensional mathematical model are:

- Mass conservation for the oil phase:

$$\frac{\partial}{\partial t}\left(m\rho_o s_o\right)+\frac{\partial}{\partial x}\left(\rho_o u_o\right)=0 \quad (1)$$

- Mass conservation for the water phase:

$$\frac{\partial}{\partial t}\left(m\rho_w s_w\right)+\frac{\partial}{\partial x}\left(\rho_w u_w\right)=0 \quad (2)$$

- Dependency of porosity:

$$m = m_0 + \beta_m \left(p - p_0\right) \quad (3)$$

- Dependencies of phase densities:

$$\rho_o = \left(\rho_o\right)_0 [1 + \beta_o \left(p - p_0\right)], \quad (4)$$

$$\rho_w = \left(\rho_w\right)_0 [1 + \beta_w \left(p - p_0\right)]; \quad (5)$$

- Phase velocities from Darcy's law:

$$u_o = -\frac{Kk_o}{\mu_o}\frac{\partial p}{\partial x}, \quad u_w = -\frac{Kk_w}{\mu_w}\frac{\partial p}{\partial x}; \tag{6}$$

- Dependency of absolute permeability:

$$K = K_0\left(\frac{m}{m_0}\right)^n; \tag{7}$$

Since the sum phase saturations equals to 1:

$$s_o + s_w = 1. \tag{8}$$

where μ_o and μ_w are taken as constants.

The relative permeability functions are given by:

$$k_o = \begin{cases}\left(\dfrac{1-s_w}{1-s_{wE}}\right), & s_w > s_{wE},\\ 1 & s_w \le s_{wE},\end{cases} \tag{9}$$

$$k_w = \begin{cases}\left(\dfrac{s_w - s_{wE}}{1-s_{wE}}\right), & s_w > s_{wE},\\ 0 & s_w \le s_{wE}.\end{cases} \tag{10}$$

where s_{wE} denotes the residual water saturation.

Rewriting (1) and (2), yields:

$$\rho_o s_o \frac{\partial m}{\partial t} + m\frac{\partial(\rho_o s_o)}{\partial t} + \frac{\partial(\rho_o u_o)}{\partial x} = 0 \tag{11}$$

$$\rho_w s_w \frac{\partial m}{\partial t} + m\frac{\partial(\rho_w s_w)}{\partial t} + \frac{\partial(\rho_w u_w)}{\partial x} = 0 \tag{12}$$

To derive the piezo-conductivity equation, (11) and (12) are added:

$$\begin{aligned}&(\rho_o s_o + \rho_w s_w)\frac{\partial m}{\partial t} + m\frac{\partial}{\partial t}(\rho_o s_o + \rho_w s_w)\\ &\quad + \frac{\partial}{\partial x}(\rho_o u_o + \rho_w u_w) = 0\end{aligned} \tag{13}$$

Using (3) and (6) we get:

$$\begin{aligned}&\beta_m(\rho_o s_o + \rho_w s_w)\frac{\partial p}{\partial t} =\\ &\frac{\partial}{\partial x}\left[\left(\frac{K\rho_o k_o}{\mu_o} + \frac{K\rho_w k_w}{\mu_w}\right)\frac{\partial p}{\partial x}\right]\\ &-m\frac{\partial}{\partial t}(\rho_o s_o + \rho_w s_w) = 0\end{aligned} \tag{14}$$

The initial conditions are:

$$\begin{aligned}&p(x,0) = p^0,\ m(x,0) = m_0,\ \rho_o(x,0) = (\rho_o)_0,\\ &\rho_w(x,0) = (\rho_w)_0,\ K(x,0) = K_0,\\ &s_o(x,0) = s_o^0,\ s_w(x,0) = s_w^0\end{aligned} \tag{15}$$

and the boundary conditions are:

$$p(t,0) = p^0, \quad p(t,L) = p^*, \quad p^* < p_0; \tag{16}$$

The parameter sets used in the numerical experiments were chosen to represent realistic reservoir conditions. In particular, the initial porosity value $m_0 = 0.23$ and the initial absolute permeability $K_0 = 10^{-15} m^2$ corresponded to reservoir rocks that combine relatively high total porosity with limited matrix permeability. Such porosity-permeability combinations were reported in [20-22]. This case was included as an end-member in sensitivity tests to demonstrate how deformation and pressure depletion can affect both porosity and permeability in low-transmissibility media. All other parameter values (densities, viscosities, initial pressures, compressibility coefficients) were selected within ranges typical for hydrocarbon reservoirs, as presented in Table I.

TABLE I. TYPICAL FIELD PARAMETER RANGES

Parameter	Typical range	Comment
Porosity, m	0.1-0.3	Reef carbonates and good sandstones up to 25-30%; consolidated/tight sands
Permeability, K	10^{-16} – $5\cdot10^{-13}$	Low-transmissibility matrix (0.1-1 mD) to high-quality reservoirs
Oil density, ρ_o	850-950 kg m^{-3}	Light-to-medium crude typical for the region
Water density, ρ_w	1000 kg m^{-3}	Brine
Oil viscosity, μ_o	$2\cdot10^{-3}$ – 10^{-2} Pa·s	Depends on API; used for sensitivity cases
Reservoir pressure, p	5-30 MPa	Typical for depths ~1-3 km
Medium compressibility, β_m	10^{-9} – 10^{-8} Pa^{-1}	Consolidated sandstones, carbonates

III. SOLUTION ALGORITHM

Equations (1) - (16) were solved using the "large particle" method. Initially, the following Euler's grid was introduced [19]:

$$\begin{aligned}&\Omega_{\tau h} = \Big\{\ t_{k+1} = t_k + \tau,\ \ j = 0,..,N_t - 1;\ j = \frac{T}{N_t};\\ &x_{i+1} = x_i + h,\ i = 0,..,N_x - 1;\ i = \frac{L}{N_x}\Big\},\end{aligned} \tag{17}$$

The environment was modeled as a system of liquid particles that coincide at a given moment in time with a cell of the Euler grid. The calculation of each time step was divided into three stages:

- Stage 1: Neglecting the effects associated with the displacement of the unit cell, (14) was approximated at time t_k:

$$\beta_m \left(\rho_o s_o + \rho_w s_w\right)_i^k \frac{\tilde{p}_i - p_i^k}{\tau} = \frac{1}{h^2}\left\{b^k_{i-\frac{1}{2}}\tilde{p}_{i-1} - \left(b^k_{i-\frac{1}{2}} + b^k_{i+\frac{1}{2}}\right)\tilde{p}_i + b^k_{i+\frac{1}{2}}\tilde{p}_{i+1}\right\} - m_i^k \frac{\left(\rho_o s_o + \rho_w s_w\right)_i^k - \left(\rho_o s_o + \rho_w s_w\right)_i^{k-1}}{\tau}, \quad (18)$$

where:

$$b_i^k = \left[K\left(\frac{\rho_o k_o}{\mu_o} + \frac{\rho_w k_w}{\mu_w}\right)\right]_i^k \quad (19)$$

To solve the linear system, (18) was rewritten in the following form:

$$A_i \tilde{p}_{i-1} - B_i \tilde{p}_i + C_i \tilde{p}_{i+1} = -F_i; \quad (20)$$

where,

$$A_i = \frac{\tau}{\beta_m \left(\rho_o s_o + \rho_w s_w\right)_i^k h^2} b^k_{i-\frac{1}{2}}$$

$$B_i = 1 + \frac{\tau}{\beta_m \left(\rho_o s_o + \rho_w s_w\right)_i^k h^2}\left\{b^k_{i-\frac{1}{2}} + b^k_{i+\frac{1}{2}}\right\} \quad (21)$$

$$C_i = \frac{\tau}{\beta_m \left(\rho_o s_o + \rho_w s_w\right)_i^k h^2} b^k_{i+\frac{1}{2}}$$

If $k = 0$, then $F_i = p_i^k$,

If $k \neq 0$, then

$$F_i = p_i^k - m_i^k \frac{\left(\rho_o s_o + \rho_w s_w\right)_i^k - \left(\rho_o s_o + \rho_w s_w\right)_i^{k-1}}{\beta_m \left(\rho_o s_o + \rho_w s_w\right)_i^{k+1}}.$$

The approximations of the initial and boundary conditions were given by:

$$p_i^0 = p^0, \quad m_i^0 = m_0, \quad \left(\rho_o\right)_i^0 = \left(\rho_o\right)_0, \quad \left(\rho_w\right)_i^0 = \left(\rho_w\right)_0, \quad K_i^0 = K_0, \quad \left(s_o\right)_i^0 = s_o^0, \quad \left(s_w\right)_i^0 = s_w^0, \quad (22)$$

$$p_0^k = p^0, \quad p_{N_x}^k = p^* \quad (23)$$

In order to solve (19), Thomas' algorithm was used [19]. The algorithm coefficients were calculated from:

$$\begin{cases} \alpha_{i+1} = \dfrac{C_i}{B_i - A_i\alpha_i}, \\ \beta_{i+1} = \dfrac{F_i + A_i\beta_i}{B_i - A_i\alpha_i} \end{cases} \quad \text{at} \quad i = \overline{1, N-1}, \quad (24)$$

and reservoir pressure was calculated according to:

$$p_i^{\sim} = \alpha_{i+1} p_{i+1}^{\sim} + \beta_{i+1}. \quad (25)$$

From the boundary conditions, it was determined that:

$$\alpha_1 = 1, \quad \beta_1 = 0, \quad p_N^{\sim} = p^*. \quad (26)$$

- Stage 2: Once the pressure values were obtained, the phase velocities were calculated using:

$$\left(u_o\right)_{i+\frac{1}{2}}^{\sim} = -\left(\frac{Kk_o}{\mu_o}\right)_i^{\sim} \frac{p_i^{\sim} - p_{i+1}^{\sim}}{h}, \quad \left(u_w\right)_{i+\frac{1}{2}}^{\sim} = -\left(\frac{Kk_w}{\mu_w}\right)_i^{\sim} \frac{p_i^{\sim} - p_{i+1}^{\sim}}{h} \quad (27)$$

- Stage 3: Using the equations of state and conservation laws, phase densities and saturations were updated from:

$$m_i^{k+1} = m_0 + \beta_m\left(p_i^{\sim} - p_0\right) \quad (28)$$

$$\left(\rho_o\right)_i^{k+1} = \left(\rho_o\right)_0 [1 + \beta_o\left(\tilde{p}_i - p_0\right)] \quad (29)$$

$$\left(\rho_w\right)_i^{k+1} = \left(\rho_w\right)_0 [1 + \beta_w\left(\tilde{p}_i - p_0\right)] \quad (30)$$

$$\left(s_w\right)_i^{k+1} = \frac{1}{\left(m\rho_w\right)_i^{k+1}} \left[\left(m\rho_w s_w\right)_i^k + \frac{\left(\rho_w\right)_i^{k+1}\left(\tilde{u}_w\right)_{i-1/2} - \left(\rho_w\right)_{i+1}^{k+1}\left(\tilde{u}_w\right)_{i+1/2}}{h}\tau\right], \quad (31)$$

$$\left(s_w\right)_i^{k+1} = 1 - \left(s_w\right)_i^{k+1}, \quad (32)$$

$$\left(k_o\right)_i^{k+1} = \begin{cases} \left(\dfrac{1 - \left(s_w\right)_i^{k+1}}{1 - s_{wE}}\right), & \left(s_w\right)_i^{k+1} > s_{wE}, \\ 1, & \left(s_w\right)_i^{k+1} \leq s_{wE}, \end{cases} \quad (33)$$

$$\left(k_w\right)_i^{k+1} = \begin{cases} \left(\dfrac{\left(s_w\right)_i^{k+1} - s_{wE}}{1 - s_{wE}}\right), & \left(s_w\right)_i^{k+1} > s_{wE}, \\ 0, & \left(s_w\right)_i^{k+1} \leq s_{wE}, \end{cases} \quad (34)$$

$$K_i^{j+1} = K_0\left[1 - a_K\left(p_0 - p_i^{\sim}\right)\right]. \quad (35)$$

IV. RESULTS AND DISCUSSION

To study the deformation of a saturated porous medium, computational experiments were carried out using the following parameter values: m_o= 0.23, K_o= $5 \cdot 10^{-15}$ m^2, s_o^0 = 0.6, s_w^0 = 0.4, p_o^0 = 10^5 Pa, p_w^0 = 10^5 Pa, p^*= =$5 \cdot 10^5$ Pa, $(p_o)^0$ = 950 kg·m^{-3}, $(p_w)^0$ = 1,002 kg·m^{-3}, μ_o = $2.23 \cdot 10^{-3}$ Pa·s, μ_w = 10^{-3} Pa·s, β_m= 10^{-8} Pa^{-1}, a_K = $-1.25 \cdot 10^{-6}$ Pa^{-1}, and T = 1 yr.

The initial reservoir and well pressures were set to $p_o^0 = 10^5\ Pa$ and $p_w^0 = 10^5\ Pa$, respectively. Figures 1(a) - 1(c) illustrate the pressure distribution for three media with different compressible coefficients. As the filtration process proceeded, the reservoir pressure decreased with time. Additionally, Figure

2 depicts the oil phase velocity profiles at different values of the compressibility coefficient at several time moments. In all cases, the velocity reached its maximum near the wellbore and decreased over time. In less compressible media, the velocity near the wellbore decreased more slowly, while the velocity in the far-field region increased due to the development of a stronger pressure gradient away from the well.

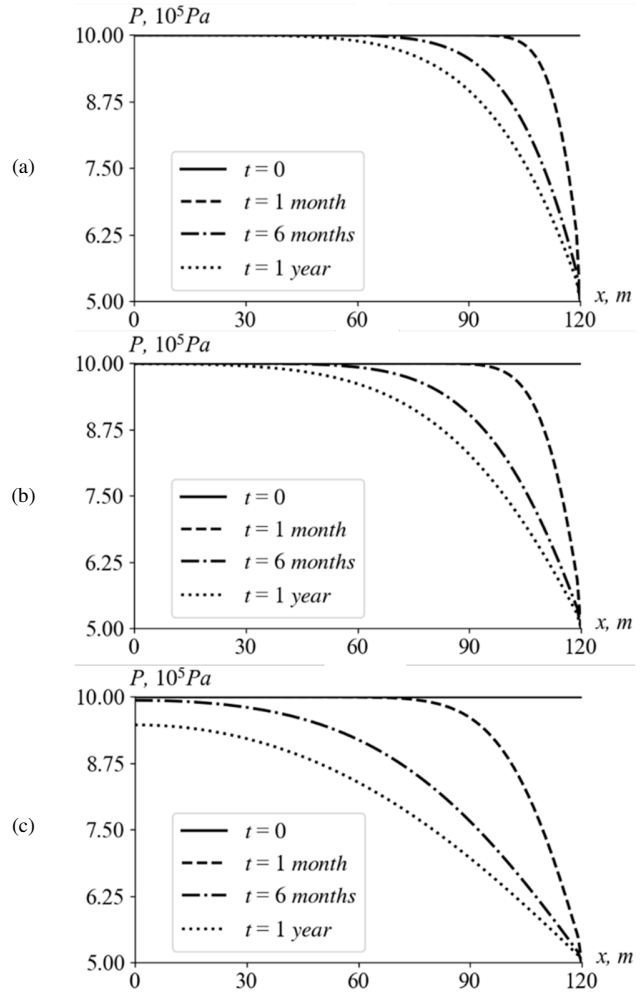

Fig. 1. Reservoir pressure profiles at (a) $\beta_m = 5 \cdot 10^{-1} Pa^{-1}$, (b) $\beta_m = 3 \cdot 10^{-1} Pa^{-1}$, and (c) $\beta_m = 10^{-1} Pa^{-1}$.

The decrease of β_m in Figure 1 led to intensification of pressure drop. This occurred because lower compressibility slowed the reduction of porosity (Figure 3) and permeability (Figure 4), thereby preserving better flow capacity. As a result, filtration remained more effective in low compressible media, leading to a faster decrease in reservoir pressure.

The decrease in the compressibility factor caused a decline in velocity in bottom-hole zone, while a rise occurred in regions far from the well. This is affected by the pressure gradient, which decreased by lowering the medium compressibility in bottom-hole zone, while arose in regions far from the well (Figure 1) in low compressible media.

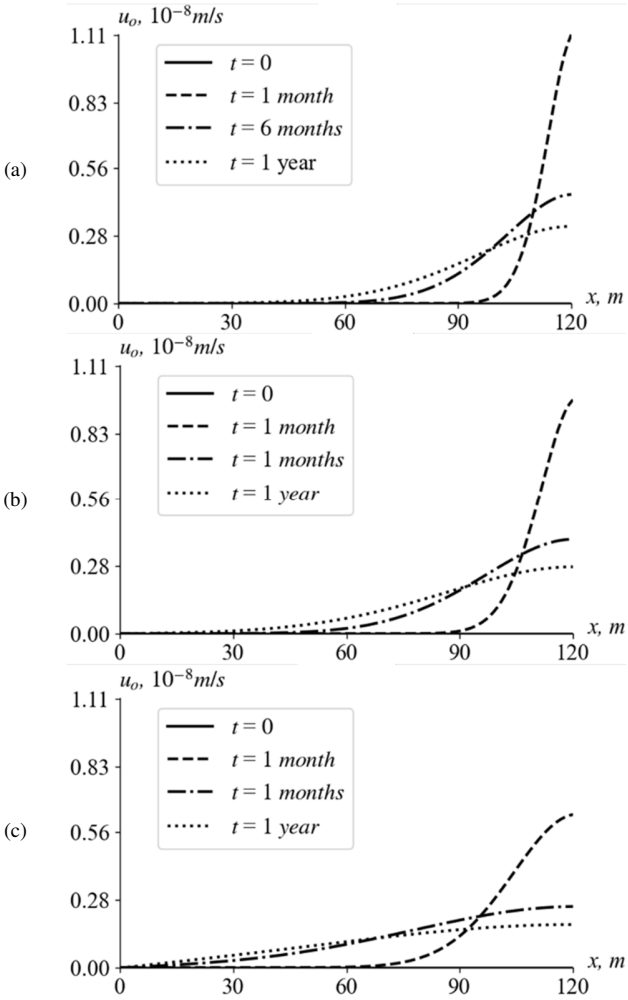

Fig. 2. Profiles of oil phase velocity at (a) $\beta_m = 5 \cdot 10^{-1} Pa^{-1}$, (b) $\beta_m = 3 \cdot 10^{-1} Pa^{-1}$, and (c) $\beta_m = 10^{-1} Pa^{-1}$.

Figures 3 and 4 present the porosity and permeability profiles at three compressibility coefficient values at different time moments. In Figures 3(a) and 4(a), porosity and permeability decline sharply in the bottom-hole zone, reaching values of $m = 0.205$ and $K = 0.56 \cdot 10^{-15} m^2$, respectively. As a result, the liquids' motion did not start in regions far from the well (Figures 1(a) and 2(a)), and porosity and permeability remained unchanged there. As compressibility decreased (Figures 3(b), 3(c), 4(b), and 4(c)), the reduction in both porosity and permeability slowed down in bottom-hole zone. However, since liquid flow extended farther into the reservoir under these conditions, porosity and permeability also decreased (Figures 3(c) and 4(c)).

To validate the results, a comparison was carried out with previously published data. Authors in [11] calculated the average pore pressure in the reservoir, pore pressure fields, subsidence, and compaction. Using the initial data from this study, calculations were performed through the proposed methodology. Table II demonstrates the average pressure

decline obtained in [11] using the two-way coupled scheme and the results obtained in this study.

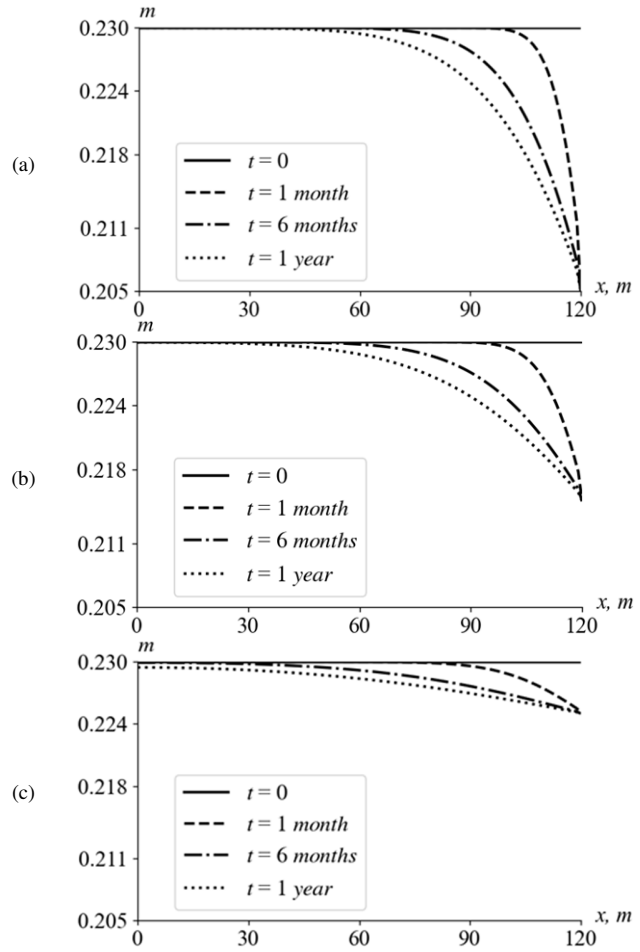

Fig. 3. Porosity profiles at (a) $\beta_m = 5 \cdot 10^{-1} Pa^{-1}$, (b) $\beta_m = 3 \cdot 10^{-1} Pa^{-1}$, and (c) $\beta_m = 10^{-1} Pa^{-1}$.

TABLE II. COMPARISON TABLE OF PREVIOUS AND PRESENT RESULTS FOR VALIDATION PURPOSES

Time	Average pressure obtained in [11], MPa	Average pressure obtained in this study, MPa
0	1	1
3 months	0.9627	0.9412
6 months	0.8908	0.8904
9 months	0.8198	0.8501
1 year	0.7616	0.8006

The maximum relative difference between the average pressures (4.8%) lays within expected numerical and modeling discrepancies given the different numerical schemes and assumptions. The important physical agreement is that both approaches predicted significant compaction and permeability reduction in the production zone under pressure depletion, and a slowing of the pressure decline as permeability and porosity collapsed locally -which confirmed the physical relevance of the current results. The present method, thus, provided comparable predictions for the average pressure and compaction while offering a computationally efficient alternative; nevertheless, differences at the 1-5% level reflect model formulation and discretization choices rather than a physical inconsistency.

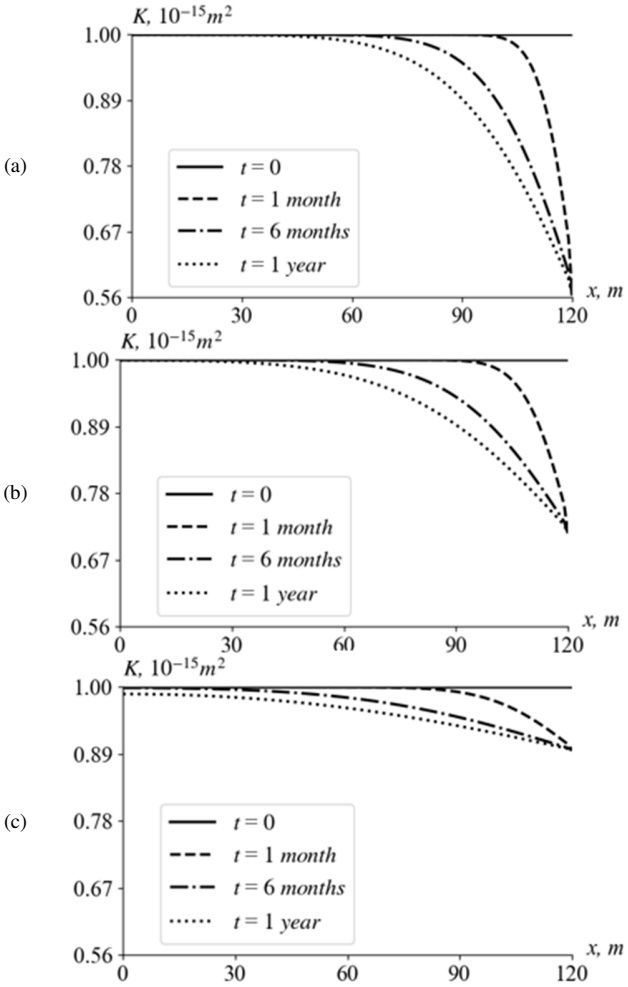

Fig. 4. Permeability profiles at (a) $\beta_m = 5 \cdot 10^{-1} Pa^{-1}$, (b) $\beta_m = 3 \cdot 10^{-1} Pa^{-1}$, and (c) $\beta_m = 10^{-1} Pa^{-1}$.

V. CONCLUSION

In this study, a one-dimensional mathematical model was developed considering medium and phase compressibility for the filtration of oil and water in an oil reservoir containing a single production well. The "large particle" method was used to obtain numerical solutions and parameters including pressure, velocity, porosity, and permeability were analyzed. The results showed that the compressibility coefficient directly affected the porosity of the medium. Higher compressibility led to a sharp decrease in porosity in bottom-hole zone, which in turn caused a reduction in permeability. These losses resulted in slower decline in reservoir pressure as well as delaying the flow of the phases in far zones from the production well.

From an applied perspective, the obtained results can be applied in the rapid screening of compaction and permeability-loss risk near production wells, especially in reservoirs with high total porosity but restricted pore-throat connectivity (e.g., vuggy carbonates or diagenetically altered sandstones). The sensitivity tests can, therefore, help operators and modelers to assess production decline scenarios and plan mitigation under realistic field parameter ranges.

NOMENCLATURE

m = porosity of the medium
ρ_o = density of oil phase
ρ_w = density of water phase
s_o = saturation of oil phase
s_w = saturation of water phase
u_o = velocity of oil phase
u_w = velocity of water phase
m_0 = initial porosity
β_m = compressibility coefficient of the medium
p_0 = reservoir pressure which the system stays under equilibrium
$(\rho_o)_0$ = initial oil density
$(\rho_w)_0$ = initial water density
β_o = compressibility coefficient of oil phase
β_w = compressibility coefficient of water phase
k_o = relative permeability of the medium to the oil phase
k_w = relative permeability of the medium to the water phase
K_0 = initial absolute permeability
a_K = permeability coefficient
p^0 = initial reservoir pressure
s_o^0 = initial oil saturation
s_w^0 = initial water saturation
p^* = well pressure
L = length of element
h = grid step in space
τ = grid step in time
N_x = number of nodes in space
N_t = number of nodes in time
L = element length
T = maximum time under consideration
o = oil phase
w = water phase

REFERENCES

[1] E. Romenski and E. F. Toro, "Compressible two-phase flows: two-pressure models and numerical methods," *Computational Fluid Dynamics Journal*, vol. 13, no. 03, pp. 403–416, 2004.

[2] S. Olivella, J. Carrera, A. Gens, and E. E. Alonso, "Nonisothermal multiphase flow of brine and gas through saline media," *Transport in Porous Media*, vol. 15, no. 3, pp. 271–293, June 1994, https://doi.org/10.1007/BF00613282.

[3] D. A. Drew and R. T. Lahey, "The virtual mass and lift force on a sphere in rotating and straining inviscid flow," *International Journal of Multiphase Flow*, vol. 13, no. 1, pp. 113–121, Jan. 1987, https://doi.org/10.1016/0301-9322(87)90011-5.

[4] M. R. Baer and J. W. Nunziato, "A two-phase mixture theory for the deflagration-to-detonation transition (ddt) in reactive granular materials," *International Journal of Multiphase Flow*, vol. 12, no. 6, pp. 861–889, Nov. 1986, https://doi.org/10.1016/0301-9322(86)90033-9.

[5] A. I. Sukhinov, L. A. Grigoryan, and A. A. Sukhinov, "Mathematical modeling of two-phase compressible fluid filtration based on modified adaptive method of minimum amendments," *Advanced Engineering Research (Rostov-on-Don)*, vol. 16, no. 3, pp. 96–109, Sept. 2016, https://doi.org/10.12737/20944.

[6] S. M. A. Ghaly, M. O. Khan, M. Shalaby, K. A. Alsnaie, and M. Oraiqat, "Real Time Measurement of Multiphase Flow Velocity using Electrical Capacitance Tomography," *Engineering, Technology & Applied Science Research*, vol. 13, no. 5, pp. 11685–11690, Oct. 2023, https://doi.org/10.48084/etasr.6130.

[7] V. Burnashev, U. Nazarov, H. Akhadkulov, M. Shodmonqulov, and J. Haydarov, "Numerical Study of Detonation Waves in Gas Suspensions with Spatially Inhomogeneous Particle Concentration Distribution in Sharply Expanding Pipes," *Journal of Advanced Research in Fluid Mechanics and Thermal Sciences*, vol. 123, no. 1, pp. 41–52, Oct. 2024, https://doi.org/10.37934/arfmts.123.1.4152.

[8] X. Mou and Z. Chen, "Pore-scale simulation of heat and mass transfer in deformable porous media," *International Journal of Heat and Mass Transfer*, vol. 158, Sept. 2020, Art. no. 119878, https://doi.org/10.1016/j.ijheatmasstransfer.2020.119878.

[9] S. Barry, G. Aldis, and G. Mercer, "Injection of Fluid Into a Layer of Deformable Porous Medium," *Applied Mechanics Reviews*, vol. 48, no. 10, pp. 722–726, Oct. 1995, https://doi.org/10.1115/1.3005054.

[10] N. T. Azhikhanov, B. T. Zhumagulov, Z. K. Masanov, and A. B. Bekbolatov, "Finite element modeling of fluid filtration in a deformable porous medium," in *Modelling and Methods of Structural Analysis*, Moscow, Russia, Nov. 2019, https://doi.org/10.1088/1742-6596/1425/1/012137.

[11] N. Inoue and S. A. B. da Fontoura, "Answers to Some Questions About the Coupling Between Fluid Flow and Rock Deformation in Oil Reservoirs," in *SPE/EAGE Reservoir Characterization and Simulation Conference*, Abu Dhabi, UAE, Oct. 2009, https://doi.org/10.2118/125760-MS.

[12] M. A. Tokareva, "On the Solvability of the Problem of Fluid Filtration in a Deformable Porous Medium in the Gravitational Field," *Altai State University News. Mathematics and Mechanics*, vol. 102, no. 4, pp. 108–113, Sept. 2018, https://doi.org/10.14258/izvasu(2018)4-20.

[13] S. Peters, Y. Heider, and B. Markert, "Numerical simulation of miscible multiphase flow and fluid–fluid interaction in deformable porous media," *Proceedings in Applied Mathematics and Mechanics (PAMM)*, vol. 23, no. 2, Sept. 2023, Art. no. e202300209, https://doi.org/10.1002/pamm.202300209.

[14] P. V. Trusov, N. V. Zaitseva, and M. Y. Tsinker, "On modeling of airflow in human lungs: constitutive relations to describe deformation of porous medium," *PNRPU Mechanics Bulletin*, no. 4, pp. 165–174, Dec. 2020, https://doi.org/10.15593/perm.mech/2020.4.14.

[15] R. A. Virts, "Numerical Solution of a Two-Dimensional Problem of Fluid Filtration in a Deformable Porous Medium," *Altai State University News. Mathematics and Mechanics*, vol. 117, no. 1, pp. 88–92, 2021.

[16] J. Abou-Kassem, M. R. Islam, and S. M. F. Ali, *Petroleum Reservoir Simulation: The Engineering Approach*. Amsterdam, Netherlands: Elsevier, 2020.

[17] A. R. Khoei and S. Saeedmonir, "Computational homogenization of fully coupled multiphase flow in deformable porous media," *Computer Methods in Applied Mechanics and Engineering*, vol. 376, Apr. 2021, Art. no. 113660, https://doi.org/10.1016/j.cma.2020.113660.

[18] S. Samimi and A. Pak, "A three-dimensional mesh-free model for analyzing multi-phase flow in deforming porous media," *Meccanica*,

vol. 51, no. 3, pp. 517–536, June 2015, https://doi.org/10.1007/s11012-015-0231-z.

[19] V. Burnashev, Z. Kaytarov, J. Tuygunov, and O. Kosimov, "A mathematical model of two-phase filtration in a porous medium taking into account its deformation," in *International Scientific and Practical Conference on Actual Problems of Mathematical Modeling and Information Technology*, Nukus, Uzbekistan, May 2023, https://doi.org/10.1063/5.0210387.

[20] F. J. Lucia, C. Kerans, and J. W. Jennings Jr., "Carbonate Reservoir Characterization," *Journal of Petroleum Technology*, vol. 55, no. 06, pp. 70–72, June 2003, https://doi.org/10.2118/82071-JPT.

[21] P. H. Nelson, "Permeability-porosity Relationships In Sedimentary Rocks," *The Log Analyst*, vol. 35, no. 03, May 1994.

[22] G. F. Ulmishek, "Petroleum geology and resources of the North Ustyurt Basin, Kazakhstan and Uzbekistan," U.S. Geological Survey, 2201-D, 2001. https://doi.org/10.3133/b2201D.